nature communications

Article

https://doi.org/10.1038/s41467-025-60826-x

Single particle fluorescence imaging of perovskite nanocrystal crystallization for illustrating coupled nucleation-and-growth

Received: 26 February 2024

Accepted: 4 June 2025

Published online: 01 July 2025

Check for updates

Lige Liu[1,2,11], Dashan Dong[1,2,3,11], Zhiwei Long[4,8], Wanxue Wei[1,2], Chang Sun[1,9], Wei Liu[1,10], Xiaoshuai Huang[5], Liangyi Chen[6], Haizheng Zhong[4] ✉ & Kebin Shi[1,2,7] ✉

Because of the lack of spatiotemporal characterization techniques, it has been of great challenge to investigate the crystallization of nanocrystals. With a high-speed structured illumination super-resolution fluorescence microscopy (SIM), we hereby report an in situ fluorescence imaging technique to monitor the crystallization of perovskite nanocrystals at single-particle level. By correlating the fluorescence intensity with particle size, we illustrate the coupled nucleation-and-growth of perovskite nanocrystals in polymer matrix. The temporal fluorescence intensity analysis of individual nanocrystals reveals the diffusion-controlled growth process with a fast growth at the beginning followed by a slow growth. The analysis of ensemble nanocrystals illustrates the evolution of nucleation rate with the change of precursor concentrations. We further analyze the Gibbs free energy fluctuation of couple nucleation-and-growth. The growth free energy dominates in the continuous nucleation of perovskite nanocrystals, which accounts for the narrow size distribution. In comparison with LaMer model, the coupled nucleation-and-growth provides an alternative model to fabricate narrow sized nanocrystals.

Since the discovery of the quantum dots (also known as semiconductor nanocrystals), size-dependence is a fundamental feature in determining their physical properties which strongly affects the subsequent processing capability and performance in different applications[1,2]. Size control, including size and size distribution, has been one of the most considerable targets in nanocrystal synthesis[3–5]. After years of efforts, it has been known that nanocrystal crystallization usually experiences nucleation and growth processes[6,7]. The key challenge is how to control the nucleation and growth. Based on the size-focusing effects in LaMer and Sugimoto models, the time separation of nucleation and growth is an effective strategy to synthesize size-tunable nanocrystals with narrow size distribution[8–11]. The narrow size distribution of nanocrystals can be explained to the size-dependent growth rate following by a burst nucleation[12–14]. Very recently, it was found that narrow size distribution could also be achieved from a continuous nucleation process with coupled

[1]State Key Laboratory of Mesoscopic Physics and Frontiers Science Center for Nano-optoelectronics, School of Physics, Peking University, Beijing, China. [2]Collaborative Innovation Center of Extreme Optics, Shanxi University, Taiyuan, China. [3]National Biomedical Imaging Center, Peking University, Beijing, China. [4]MIIT Key Laboratory for Low-dimensional Quantum Structure and Devices, School of Materials Science & Engineering, Beijing Institute of Technology, Beijing, China. [5]Biomedical Engineering Department, Peking University, Beijing, China. [6]State Key Laboratory of Membrane Biology, Beijing Key Laboratory of Cardiometabolic Molecular Medicine, Institute of Molecular Medicine, Center for Life Sciences, College of Future Technology, Peking University, Beijing, China. [7]Peking University Yangtze Delta Institute of Optoelectronics, Nantong, China. [8]Present address: Department of Electrical and Electronic Engineering, The University of Hong Kong, Hong Kong, China. [9]Present address: Research Institute for Frontier Science, Beihang University, Beijing, China. [10]Present address: Aerospace Information Research Institute, Chinese Academy of Sciences, Beijing, China. [11]These authors contributed equally: Lige Liu, Dashan Dong. ✉e-mail: hzzhong@bit.edu.cn; kebinshi@pku.edu.cn

nucleation and growth[15,16]. Therefore, separated nucleation-and-growth is not necessary to achieve narrow size distribution. This conflict inspires the experimental and theoretical study of the coupling between nucleation and growth in continuous nucleation process.

Perovskite nanocrystals are emerging as functional materials with promising future in the applications of lighting display, scintillator and quantum light source due to their superior optical properties and easy in situ fabrication[17–21]. Considering that halide perovskites are ionic compounds, the formation of perovskite nanocrystal is usually achieved via a rapid crystallization process within a few seconds to minutes, which includes coupled nucleation-and-growth[22,23]. Super-resolution fluorescence microscopy is a powerful tool to obtain fluorescence images with high spatial and temporal resolution[24,25], which is able to monitor the perovskite crystallization process at single-particle level. Compared with techniques of liquid-phase transmission electron microscope (LP-TEM) and synchrotron X-ray scattering measurements, which are two important techniques for in situ characterizing the crystallization of nanocrystals[26,27], optical imaging is a lab affordable technique to bridge the large-scale equipment and lab characterization.

In this work, by applying super-resolution structured illumination microscopy (SIM) technique, we show that the crystallization of perovskite nanocrystal in polymeric matrix can be in situ characterized at single-particle level. The results reveal the coupling between nucleation and growth with the simulation of kinetics and thermodynamics. Individual perovskite nanocrystals show the feature of diffusion-controlled growth, while the analysis of ensemble nanocrystals illustrate the evolution of nucleation rate. Thermodynamic simulations reveals that the free energy fluctuation of growth is dominated in the crystallization of perovskite nanocrystals.

Results and discussion

Single particle fluorescence imaging of perovskite nanocrystal crystallization

Figure 1a schematically shows the in situ experimental measurements of the crystallization of perovskite nanocrystals in polymeric matrix. A solution of perovskite precursors and poly-vinylidene difluoride (PVDF) in N, N-dimethyl formamide (DMF) was prepared and dropped onto the pre-cleaned glass substrate[28]. With the evaporation of solvent, a thin film of perovskite nanocrystals ($FAPbBr_3$, $FA = HC(NH_2)_2$) in polymer matrix was created with droplet shrinkage (Supplementary Movie 1). The fluorescence intensity in a given frame was measured by integrating the camera counts over the fluorescence emitters (Supplementary Note 1). The spatial distributions of fluorescence intensity of perovskite nanocrystals at single-particle level can be recorded on two-dimensional plane (Supplementary Movie 2). By time-lapse fluorescence imaging, the crystallization of perovskite nanocrystals can be recorded to study the nucleation and growth processes.

Figure 1b presents the high spatial resolution SIM image of perovskite nanocrystals. Single nanocrystal can be resolved from the acquired SIM image by tracking the fluorescence intensity of individual particles. We also observed fluorescent blinking of these nanocrystals with time-dependent fluorescence intensity (Supplementary Figs. 4, 5 and Movie 3). The fluorescence blinking hardly changes the overall growth time of an individual nanocrystal. The individual existence of perovskite nanocrystals in polymeric matrix was also confirmed by high-resolution TEM observation (Supplementary Fig. 6). Figure 1c shows a typical time-lapse trace of fluorescence intensity (normalized) of an individual perovskite nanocrystal. The fluorescence intensity curves of individual nanocrystals exhibit "T"-shaped curves. Figure 1d shows the time-lapse traces of normalized fluorescence intensities that summarized over a number of perovskite nanocrystals on an area of

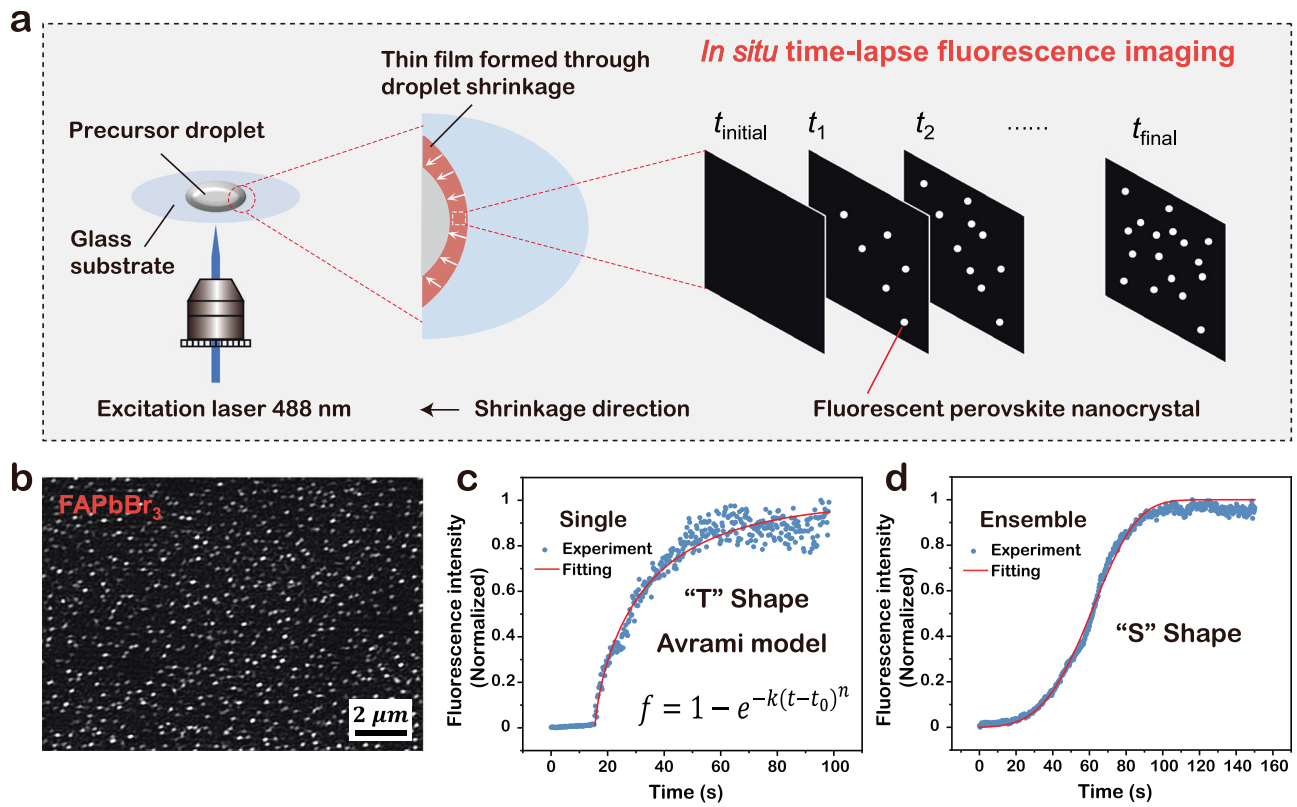

Fig. 1 | Super-resolution fluorescence imaging of perovskite nanocrystals and observation of the coupled continuous nucleation-and-growth processes. **a** Schematic illustrate the in situ crystallization of perovskite nanocrystals in polymeric matrix and time-lapse fluorescence imaging of nanocrystals with SIM. **b** Fluorescence image of perovskite nanocrystals acquired using SIM. **c**, **d** Temporal evolution of fluorescence intensity (normalized) of a bright perovskite nanocrystal and ensembles, respectively.

307 pixels × 307 pixels (10μm × 10μm). The collective fluorescence intensity curve of about 700 nanocrystals shows a feature of "S" profile. The observed "T" and "S" shaped fluorescence intensity curves are very similar with the nucleation-growth kinetic curves of Avrami model[29–31], suggesting the potential of fluorescence intensity in determine the crystallization of perovskite nanocrystals.

According to previous works, the concentration of precursors is one of the key factors affecting nucleation and growth[4,28]. In this work, we prepared three precursor solutions with different concentrations of 0.018 mol L^{-1} (C_0), 0.009 mol L^{-1} ($0.5C_0$) and 0.007 mol L^{-1} ($0.4C_0$), and we obtained three samples with different sizes. As shown in the TEM images (see below and Supplementary Fig. 6), the average diameters of the resultant perovskite nanocrystals are 3.0 ± 0.4, 4.4 ± 0.6, and 5.1 ± 0.6 nm with standard deviation (SD) of 13%, 14% and 12%, respectively. In order to determine the relationship between fluorescence intensity and nanocrystal size, the steady-state and time-resolved fluorescence spectra of perovskite nanocrystals with different sizes were measured. A mathematical expression of fluorescence intensity related with nanocrystal radius was derived (Supplementary Note 2). The relationship between fluorescence intensity and particle size was derived based on Brus equation. By using this expression, the plot of fluorescence intensity *versus* time can be transformed into nanocrystal radius versus time, enabling us to analyze the nanocrystal growth via temporal fluorescence intensity.

Crystallization, typical of first-order phase transition from solution to crystalline solid, is a complicated process with nucleation and growth stages[32,33]. The theory of crystallization can be divided into kinetics and thermodynamics. The former concerns kinetics rate of nucleation and growth, while the latter focuses on thermodynamic characteristics such as free energy and critical size. According to crystallization theory, these two stages are likely to time overlapping (coupling) with each other during formation of ensemble nanocrystals[34,35]. Based on the mathematical relationship between fluorescence intensity and nanocrystal radius, the recorded "S" shaped curve of ensemble nanocrystals shows the collective feature of perovskite formation, which illustrates the coupling between nucleation and growth. As shown in Fig. 1d, it appears as an initial slow kinetics rate then followed by a rapid crystallization that was induced by continuous nucleation and rapid growth of nanocrystals, and next the kinetics rate slows down and becomes constant with the consumption of perovskite precursors. In Fig. 1c, the "T" shaped curve of an individual nanocrystal shows the growth kinetics of a fixed nucleus beginning with a fast growth rate. We first simulate the growth kinetics of perovskite nanocrystals using traditional Avrami equation and Fick's first law-based growth model. Subsequently, a modified thermodynamics model was developed to simulate the coupling between nucleation and growth.

According to Avrami equation, nucleation and growth can be described by correlating the transformation fraction and time using Eq. (1)

$$f = 1 - e^{-k(t-t_0)^n} \quad (1)$$

where f represents volume fraction of formed crystal, k is overall crystallization rate constant and t_0 is time of initial crystallization. n represents the crystallization exponent with a wide range of values depending on nucleation rate, growth dimensionality and growth mechanisms (Supplementary Note 3). Because of the size dependent fluorescence intensity of perovskite nanocrystals, the volume fraction can be estimated by the fluorescence intensity[36]. Supplementary Fig. 10 show the fitted "S"-shaped crystallization kinetic curves of perovskite nanocrystals at different precursor concentration. The extract crystallization exponent n varied from 1.8 to 4.0, which shows the coupling between nucleation and growth of perovskite nanocrystals at different precursor concentration. $n = 4$ can be explained to the finite size effects in non-uniform nucleation, and/or three-dimensional anisotropic growth and/or size-dependent growth effect in transient nucleation[37,38]. The analysis at single-particle level can isolate growth of individual nanocrystals to illustrate the coupling between nucleation and growth. By fitting the growth kinetic curve using Avrami equation, the growth characteristics of individual nanocrystals can be obtained (Supplementary Figs. 11, 12). The extracted Avrami exponent n of 1.5 is characteristics of diffusion-controlled three-dimensional (sphere) growth.

Growth kinetics of individual nanocrystals

In situ fluorescence spectra of perovskite nanocrystals was measured by spin-coating the precursor solution on glass substrate. The SIM system can detect the signal of perovskite nanocrystals with wavelength over 500 nm. As shown in Fig. 2a, the fluorescence emission peak of perovskite nanocrystals shifts from ~500 nm to 520 nm corresponding to size increasing. Figure 2b shows the plot of the derived function relating fluorescence intensity and particle radius in a range of 0.2–3.0 nm. The temporal evolution of nanocrystal radius is in good agreement with LaMer diffusion-controlled growth theory which accounts for growth of an individual nanocrystal (Supplementary Note 4)[7,39]. Figure 2c shows the experimental temporal evolution of an individual nanocrystal radius (purple dots) and theory fitting using LaMer model (orange line). The fitting parameter of diffusion coefficient is on the order of magnitude of ~10^{-13} m^2/s (Supplementary Table 3), which is close to that of water in PVDF polymer (~10^{-12} m^2/s)[40]. Due to the existence of polymer in precursor solution, the mass diffusion rate is much slower than reported diffusion coefficient of perovskite precursors in organic solvent (~10^{-10} m^2/s)[41]. The growth of individual nanocrystals shows a fast growth at the beginning followed by a slow growth with an obvious transition of growth rate. According to Sugimoto's size-focusing theory, the narrow size distribution is significantly affected by growth kinetics. Figure 2d shows the histogram of growth time distribution of individual perovskite nanocrystals, and as observed that the fast growth process takes only a few seconds (4–8 s). After the fast growth stage, a slow growth stage was followed with time duration of tens of seconds. A few represented growth kinetics curves of individual perovskite nanocrystals with different size are provided in Supplementary Fig. 13. Based on the above results, a fast growth at the beginning followed by a slow growth is critical for the formation of monodisperse perovskite nanocrystals, even the growth is coupled with continuous nucleation. Figure 2e shows the TEM images of the perovskite nanocrystals at precursor concentration of C_0. The perovskite nanocrystals have particle size of 3.0 ± 0.4 nm with SD of 13%. The high-resolution TEM image of an individual perovskite nanocrystal presents obvious crystal lattice fringes with a spacing of 0.20 nm corresponding to (200) plane. The Fast Fourier Transform (FFT) image with obvious crystal diffraction pattern also indicates a good crystallinity of the perovskite nanocrystals.

Coupling between nucleation and growth

Figure 3a schematically illustrates the comparison between continuous nucleation and burst nucleation. Generally, nuclei start to form when the precursor solution reaches a critical concentration (minimum supersaturated concentration C^*_{min}). For burst nucleation, a large number of nuclei form at once and all the nucleus grow simultaneously to produce monodisperse particles with narrow size distribution. For continuous nucleation the nuclei number continuously increases until the solution concentration drops below the critical concentration. Once a nucleus forms it grows rapidly and then the growth rate gradually slow down. The continuous nucleation can be analyzed by counting the evolution of particle number on a specific area with time prolonging. Figure 3b shows the temporal evolution of particle numbers recorded on a fixed imaging area (10μm × 10μm) for nanocrystals

https://doi.org/10.1038/s41467-025-60826-x

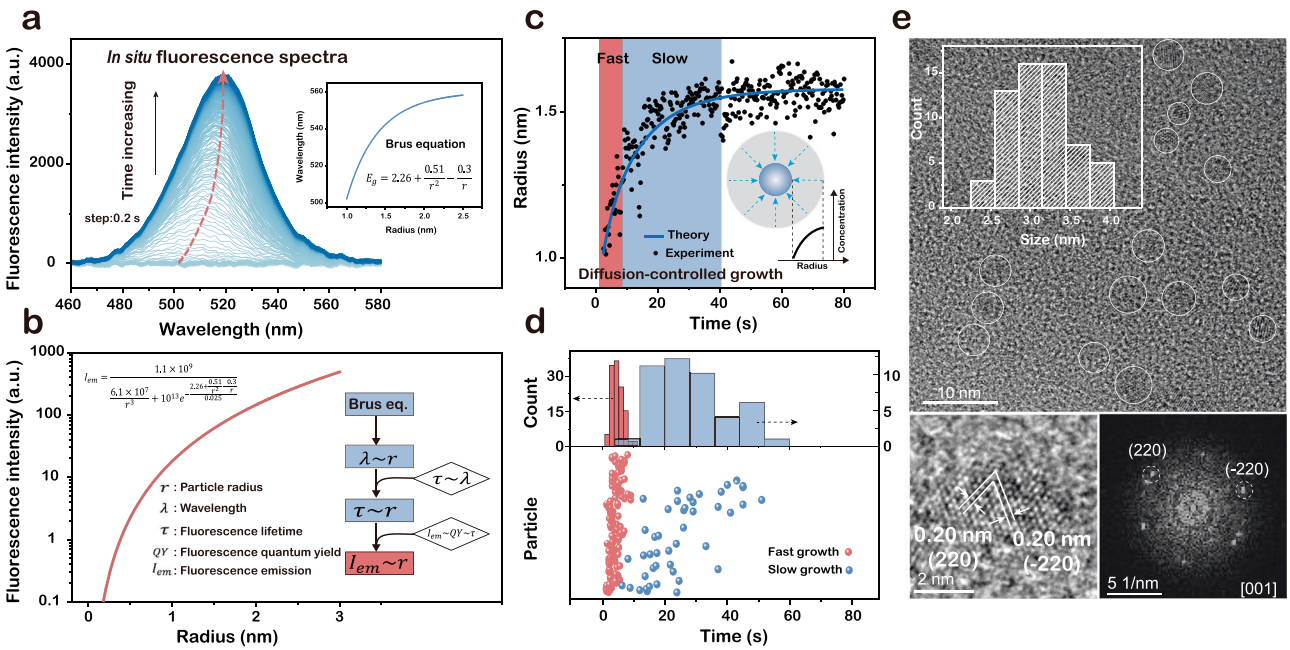

Fig. 2 | Monitoring the growth of individual perovskite nanocrystals and growth kinetics simulation. a In situ fluorescence spectra of perovskite nanocrystals in polymeric matrix. Insert is plot of Brus equation. The red line with arrow was plotted to indicate the size increasing. **b** Plot of fluorescence intensity (log) *vs.* particle radius of perovskite nanocrystal using the derived equation. Insert is flowsheet of the relationship (fluorescence intensity and particle radius) derivation. **c** Temporal evolution of an individual perovskite nanocrystal radius at precursor concentration of C_0. The blue line represents the calculated curves from the diffusion-controlled growth model. The model is schematically shown in insert. **d** Statistical histogram of the fast- and slow-growth time duration of the individual perovskite nanocrystals. 119 nanocrystals were counted. 80% of the final size was defined as the segmentation point for the fast and slow growth. **e** TEM image of the perovskite nanocrystals at precursor concentration of C_0 and histogram of the particle size distribution (insert), as well as the high-resolution TEM image of an individual perovskite nanocrystal and the corresponding FFT image.

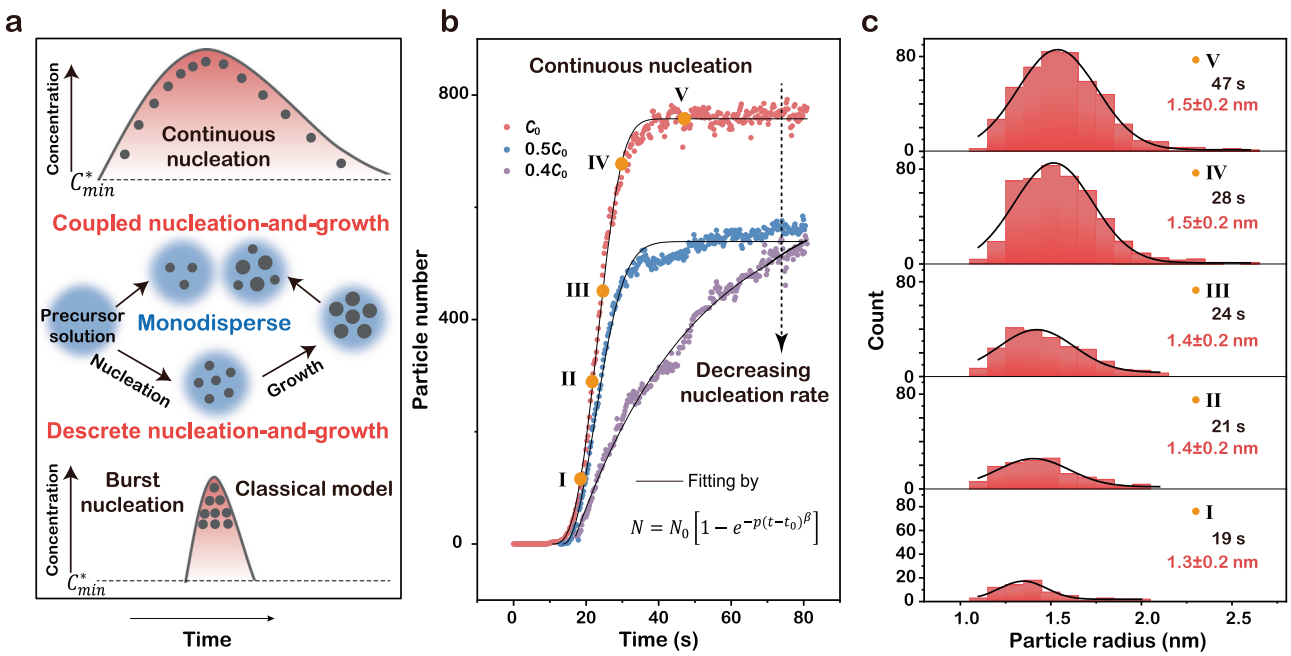

Fig. 3 | Observation of continuous nucleation and comparison with burst nucleation. a Schematic illustration of monodisperse nanocrystals with continuous nucleation and burst nucleation. **b** Temporal evolution of particle number at precursor concentration of C_0 (red line), $0.5C_0$ (blue line) and $0.4C_0$ (orange line) on an area of 307 pixels × 307 pixels (10μm × 10μm) in fluorescence images. **c** Histograms of particle radius distribution and their Gauss fitting at different nucleation time prolonging at precursor concentration of C_0.

at different precursor concentration of C_0 (red dots), $0.5C_0$ (blue dots) and $0.4C_0$ (purple dots). The nucleation kinetics can be varied by the precursor concentration. With the precursor concentration decreasing, the nucleation rate (dN/dt, N is particle number) decreases with the nucleation time increasing and the final particle number decreasing (Supplementary Note 5). In continuous nucleation of perovskite nanocrystals, the formation time of nuclei lasts for tens of seconds. The continuous nucleation of perovskite nanocrystals was also

https://doi.org/10.1038/s41467-025-60826-x

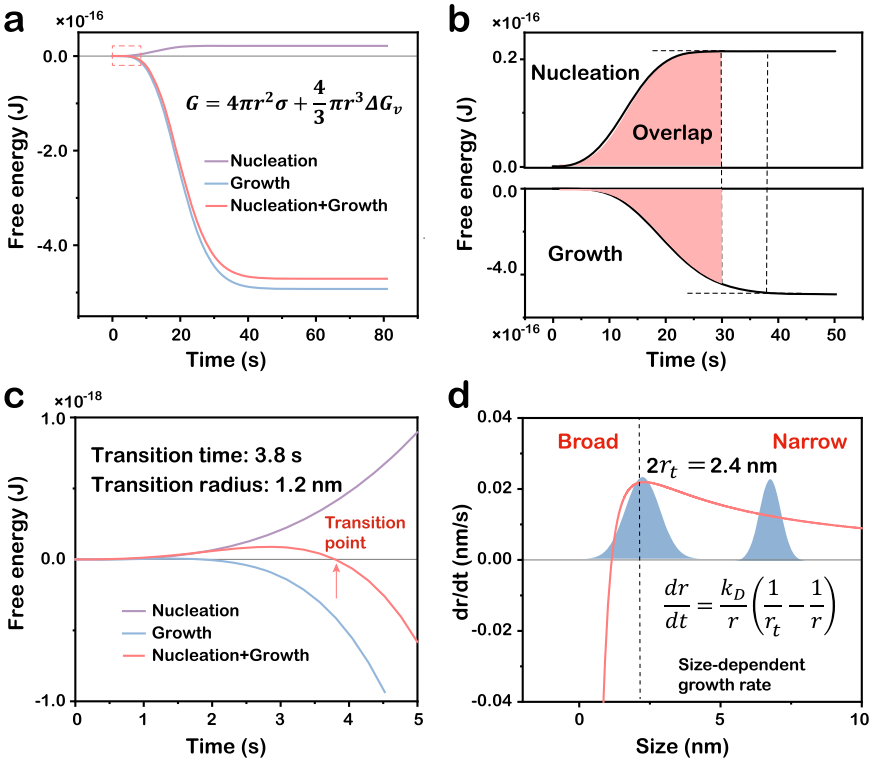

Fig. 4 | Simulation of the coupled continuous nucleation-and-growth of perovskite nanocrystals. a Temporal evolution of perovskite nanocrystal free energy at precursor concentration of C_0. Nucleation free energy (purple curve), growth free energy (blue curve) and total (mathematical sum) free energy (red curve). **b** Time overlap shows the coupling between nucleation and grow process of perovskite nanocrystals. **c** The enlarged view of the free energy curve in the red dashed frame in a. The transition size and time refer to the nanocrystal ensembles in a reaction system. **d** Diffusion-controlled growth rate (dr/dt) as a function of r with continuous nucleation of perovskite nanocrystals.

observed in a different polymeric matrix (Supplementary Note 6). Due to diffusion-controlled growth, perovskite nanocrystals can achieve nearly monodisperse size distribution. This is different from the burst nucleation of LaMer model that a large number of nuclei are initially formed, followed by a slow diffusion-controlled growth in a reaction system. Figure 3c shows that the perovskite nanocrystals have particle size distribution with SD of ~14–17% at nucleation time prolonging of 19st, 21th, 24th, 28th, and 47th second (as noted by the orange dot in Fig. 3b).

The coupling between nucleation and growth was further analyzed by simulating the temporal evolution of free energy during crystallization. According to the well-known Gibbs free energy theory, total free energy of an individual particle can be described by Eq. (2)[32,42]

$$G = 4\pi r^2\sigma + \frac{4}{3}\pi r^3 \Delta G_v \quad (2)$$

where r is the particle radius, σ is surface free energy per unit area and ΔG_v is bulk free energy per unit volume. In the crystallization process of a reaction system, the free energy of all the nanocrystals can be divided into nucleation free energy and growth free energy. The calculation of the nucleation free energy of the nanocrystals only needs to consider a fixed radius (critical nucleation radius) for all the particles even at different nucleation time prolonging. The calculation of growth free energy is more complicated because it must take into account a variety of particle sizes at each moment considering different particle size at different growth time. A mathematical model of coupled nucleation-and-growth was built and the program was accomplished on Matlab software (Supplementary Note 7). Figure 4a shows the temporal evolution of nucleation (purple curve) and growth free energy (blue curve) of the perovskite nanocrystals at precursor concentration of C_0. The nucleation free energy, as a resisting force to crystallization, is always positive and gradually rises in a "S" profile. The growth free energy is initially positive and then negative. The negative free energy is a driving force to promote nanocrystal grow into large particle. The total free energy of the nanocrystals was also plotted and as expected it shows a critical transition time/size where the total free energy value transforms from positive to negative (red curve). After the critical transition time, the nuclei number increase rapidly and the negative growth free energy dominates the total free energy. The coupling between nucleation and growth shows a time overlap of about 60% for nanocrystals at precursor concentration of C_0 as shown in Fig. 4b. With the decrease of precursor concentration, the nucleation time increases, resulting in longer time overlap between nucleation and growth (Fig. 4b and Supplementary Fig. 16). Figure 4c shows the enlarged view of the free energy curves in the dashed red frame in Fig. 4a. The total free energy has a positive-to-negative transition time at 3.8 s corresponding to a transition radius (r_t) of 1.2 nm for nanocrystal ensembles in one reaction system. After this transition point, the size distribution of the perovskite nanocrystals becomes narrower. In comparison with the free energy of continuous nucleation, the free energy of growth is dominated in the crystallization of perovskite nanocrystals.

The perovskite nanocrystals have a particle size distribution with SD < 20% (Supplementary Note 8). The narrow particle size distribution of perovskite nanocrystals in polymeric matrix was attributed to the size-dependent growth rate in diffusion-controlled growth mechanism. According to Sugimoto diffusion-controlled growth model[12], the particle size distribution becomes narrow due to the size-dependent growth rate (Supplementary Note 9). Here we simulated

the growth rate with size increasing with Eq. (3)

$$\frac{dr}{dt} = \frac{k_D}{r}\left(\frac{1}{r_t} - \frac{1}{r}\right) \quad (3)$$

where k_D is a constant for a certain concentration of precursor solution. By using the calculated k_D, the growth rate curves were calculated. Figure 4d shows the growth rate curve of perovskite nanocrystals at C_0. The growth rate decreases continuously when particle size is larger than transition radius of 1.2 nm. The smaller nanocrystals grow faster than the larger ones resulting size focusing during nanocrystal crystallization, which is in line with the Sugimoto size-focusing model. The growth dominated crystallization in coupled nucleation-and-growth process leads to particle size narrowing.

We show that super-resolution fluorescence imaging can facilitate high-spatiotemporal-resolution observation of the nucleation and growth of perovskite nanocrystal at single-particle level. The visualization of perovskite crystallization at single-particle level provides important information to isolate the growth kinetics from the coupled nucleation-and-growth. Our finding confirms that the crystallization of perovskite nanocrystals in polymeric matrix shows a typical diffusion-controlled growth with a fast growth at the beginning followed by a slow growth. For the in situ formation of perovskite nanocrystals in polymeric matrix, the nucleation time lasts for tens of seconds. With the precursor concentration decreasing, the nucleation rate decreases and nucleation time increases. By combining the experimental observation and theory simulation, we demonstrate the evolution of free energy for nucleation and growth. In the continuous nucleation of perovskite nanocrystals, free energy of growth is dominated during the crystallization process. The work not only provides a technique to illustrate the crystallization process of nanocrystals, but also describes a coupled nucleation-and-growth model to guide the optimization of nanocrystal synthesis.

Methods

Sample preparation

The perovskite precursor solution at a concentration of C_0 was prepared by mixing 0.0214 g FABr, 0.063 g $PbBr_2$, and 0.02 g C8Br [=$CH_3(CH_2)_7NH_3Br$] with 1 g PVDF polymer powder. DMF (10 mL) was added to the above mixture as solvent and stirred vigorously. The precursor solution at a concentration of $0.5C_0$ was prepared by reducing the FABr, $PbBr_2$, and C8Br and PVDF mass by half to 0.0107, 0.0315, 0.01 and 0.5 g, respectively, while maintaining the same dosage of DMF. The concentration of $0.4C_0$ precursor solution was prepared by reducing the FABr, $PbBr_2$, C8Br and PVDF mass to two-fifths the mass of FABr, $PbBr_2$, C8Br and PVDF, respectively. A drop (2 µL) of the prepared solution was dripped onto glass substrate (25-mm diameter and 170-µm thickness, Thorlabs CG15XH1) and observed through the objective lens of an inverted optical microscope. This fabrication method resulted in the generation of nano-sized $FAPbBr_3$ crystals embedded in PVDF polymeric matrix.

Characterization

TEM images were acquired using a TECNAI F20 TEM system. TEM samples were fabricated through in situ crystallization of perovskite nanocrystals on the carbon film supported by copper mesh. In details, drip a drop of perovskite precursor solution onto the copper mesh and wait for evaporation of solvent to form nanocrystals before putting them into sample room of the TEM system. Nanocrystal sizes were calculated manually using the software of "Nano Measurer". The in situ fluorescence spectra were measured during the spin-coating (4000 revolutions per minute lasts for 180 s) of the perovskite nanocrystals films at precursor concentration of C_0 on glass substrate in surrounding atmosphere. The emission signal was continuously recorded by an Ocean Optics spectrofluorometer (USB2000+) through an optical fiber. The samples were excited by a 405 nm laser coupled to another optical fiber.

Image acquisition

SIM microscopy is based on a commercially available Olympus IX83 inverted fluorescence microscope frame fitted with a 100X/NA1.45 objectives (ApoN, Olympus) immersed in oil to obtain high spatial resolution. An excitation continuous wave linearly polarized laser beam (Coherent, Sapphire 488LP-200) was spatially modulated by a spatial light modulator (QXDA-3DM, Forth Dimension Displays), generating SIM pattern illumination and projected onto an area of 108×81 μm^2 on the sample substrate with a power density of approximately 8 W cm^{-2}. A multiband dichroic filter (ZT405/488/561/640-phase R, Chroma) is used to eliminate the reflected 488 nm excitation, featuring a high transmittance of ~97% within the 500–548 nm range (Supplementary Fig. 2). The filter had minimal effect on the fluorescence spectra shape, as demonstrated in Supplementary Fig. 3. Fluorescence emission was detected using an sCMOS camera (OCRD-Flash4.0 V2, Hamamastu) with a peak quantum efficiency of 82%. Structured illumination at 488 nm was applied prior to detecting any fluorescence from nanocrystals in the field of view, enabling real-time observation of the complete crystallization process of perovskite nanocrystals. Single-particle fluorescence intensity from nanocrystals of varying particle sizes were measured under identical excitation and detection conditions, ensuring values remained within the camera's dynamic range. Fluorescence intensity emitted per particle was calculated by integrating the camera counts over each fluorescence spot. The real-time monitoring continued until no further increase in fluorescence intensity was observed in the region of interest. SIM images were post-processed and reconstructed using a modified two-step Lucy–Richardson deconvolution algorithm[43]. The resulting spatial and temporal resolution were ~100 nm and 0.238 s per frame, respectively, with a final image pixel width of 0.0325 µm.

Image data analysis and statistics

Raw images were stored in TIFF stack format. SIM images were reconstructed using custom SIM image processing software developed in MATLAB (2020a, Mathworks). Nine low-resolution fluorescence images were used to reconstruct a super-resolution image through precise mathematical deconvolution of distinct spatial frequency components under varying illumination pattern. The fluorescence intensity of single/ensemble particles was measured on output image stacks using ImageJ (Fiji) software. To calculate particle numbers, the TrackMate plugin in ImageJ (Fiji) was utilized for particle detection. All data were plotted using OriginPro (2020, OriginLab), and final images were prepared in Adobe Illustrator.

Data availability

All data supporting this study are provided in the article and the Supplementary Information file. The source data were deposited to figshare database (https://doi.org/10.6084/m9.figshare.25189316).

Code availability

All data in support of the findings of this study are available within the article and its Supplementary Information. The software supporting SIM image processing is available at https://github.com/dashandong/nanoSIM.

References

1. García de Arquer, F. P. et al. Semiconductor quantum dots: technological progress and future challenges. *Science* **373**, eaaz8541 (2021).
2. Efros, A. L. & Brus, L. E. Nanocrystal quantum dots: from discovery to modern development. *ACS Nano* **15**, 6192–6210 (2021).

3. Akkerman, Q. A. et al. Controlling the nucleation and growth kinetics of lead halide perovskite quantum dots. *Science* **377**, 1406–1412 (2022).
4. Long, Z. et al. A reactivity-controlled epitaxial growth strategy for synthesizing large nanocrystals. *Nat. Synth.* **2**, 296–304 (2023).
5. Chang, H. et al. Molecular-level understanding of continuous growth from iron-oxo clusters to iron oxide nanoparticles. *J. Am. Chem. Soc.* **141**, 7037–7045 (2019).
6. Baumgartner, J. et al. Nucleation and growth of magnetite from solution. *Nat. Mater.* **12**, 310–314 (2013).
7. Thanh, N. T. K., Maclean, N. & Mahiddine, S. Mechanisms of nucleation and growth of nanoparticles in solution. *Chem. Rev.* **114**, 7610–7630 (2014).
8. LaMer, V. K. & Dinegar, R. H. Theory, production and mechanism of formation of monodispersed hydrosols. *J. Am. Chem. Soc.* **72**, 4847–4854 (1950).
9. LaMer, V. K. Nucleation in phase transitions. *J. Ind. Eng. Chem.* **44**, 1270–1277 (1952).
10. Montanarella, F. et al. Growth and self-assembly of $CsPbBr_3$ nanocrystals in the TOPO/$PbBr_2$ synthesis as seen with x-ray scattering. *Nano Lett.* **23**, 667–676 (2023).
11. Sun, C. et al. Toward the controlled synthesis of lead halide perovskite nanocrystals. *ACS Nano* **17**, 17600–17609 (2023).
12. Sugimoto, T. Preparation of monodispersed colloidal particles. *Adv. Colloid Interface Sci.* **28**, 65–108 (1987).
13. Sugimoto, T. Underlying mechanisms in size control of uniform nanoparticles. *J. Colloid Interface Sci.* **309**, 106–118 (2007).
14. Peng, X., Wickham, J. & Alivisatos, A. P. Kinetics of II-VI and III-V colloidal semiconductor nanocrystal growth: "focusing" of size distributions. *J. Am. Chem. Soc.* **120**, 5343–5344 (1998).
15. Prins, P. T. et al. Extended nucleation and superfocusing in colloidal semiconductor nanocrystal synthesis. *Nano Lett.* **21**, 2487–2496 (2021).
16. Liu, L. et al. A general crystallization picture of quantum dots: the underlying physical chemistry. *CCS Chem.* **7**, 926–949 (2025).
17. Zhang, F. et al. Brightly luminescent and color-tunable colloidal $CH_3NH_3PbX_3$ (X= Br, I, Cl) quantum dots: potential alternatives for display technology. *ACS Nano* **9**, 4533–4542 (2015).
18. Protesescu, L. et al. Nanocrystals of cesium lead halide perovskites ($CsPbX_3$, X= Cl, Br, and I): novel optoelectronic materials showing bright emission with wide color gamut. *Nano Lett.* **15**, 3692–3696 (2015).
19. Chen, Q. et al. All-inorganic perovskite nanocrystal scintillators. *Nature* **561**, 88–93 (2018).
20. Utzat, H. et al. Coherent single-photon emission from colloidal lead halide perovskite quantum dots. *Science* **363**, 1068–1072 (2019).
21. Wu, X., Jing, Y. & Zhong, H. In situ fabricated perovskite quantum dots: from materials to applications. *Adv. Mater.* 2412276 https://doi.org/10.1002/adma.202412276 (2025).
22. Shamsi, J., Urban, A. S., Imran, M., Trizio, L. D. & Manna, L. Metal halide perovskite nanocrystals: synthesis, post-synthesis modifications, and their optical properties. *Chem. Rev.* **119**, 3296–3348 (2019).
23. Pradhan, N. Growth of lead halide perovskite nanocrystals: still in mystery. *ACS Phys. Chem. Au* **2**, 268–276 (2022).
24. Huang, X. et al. Fast, Long-term, super-resolution imaging with Hessian structured illumination microscopy. *Nat. Biotech.* **36**, 451–459 (2018).
25. Dong, D. et al. Super-resolution fluorescence-assisted diffraction computational tomography reveals the three-dimensional landscape of the cellular organelle interactome. *Light Sci. Appl.* **9**, 11 (2020).
26. Zheng, H. et al. Observation of single colloidal platinum nanocrystal growth trajectories. *Science* **324**, 1309–1312 (2009).
27. Wu, S., Li, M. & Sun, Y. In situ synchrotron X-ray characterization shining light on the nucleation and growth kinetics of colloidal nanoparticles. *Angew. Chem. Int. Ed.* **58**, 8987–8995 (2019).
28. Zhou, Q. et al. In situ fabrication of halide perovskite nanocrystal-embedded polymer composite films with enhanced photoluminescence for display backlights. *Adv. Mater.* **28**, 9163–9168 (2016).
29. Avrami, M. Kinetics of phase change. I General theory. *J. Chem. Phys.* **7**, 1103–1112 (1939).
30. Avrami, M. Kinetics of phase change. II Transformation-time relations for random distribution of nuclei. *J. Chem. Phys.* **8**, 212–224 (1940).
31. Avrami, M. Granulation, phase change and microstructure Kinetics of Phase Change. III. *J. Chem. Phys.* **9**, 177–184 (1941).
32. Oxtoby, D. W. Nucleation of first-order phase transitions. *Acc. Chem. Res.* **31**, 91–97 (1998).
33. Binder, K. Theory of first-order phase transitions. *Rep. Prog. Phys.* **50**, 783–859 (1987).
34. Chen, C. C., Herhold, A. B., Johnson, C. S. & Alivisatos, A. P. Size dependence of structural metastability in semiconductor nanocrystals. *Science* **276**, 398–401 (1997).
35. Ko, H., Sin, D. H., Kim, M. & Cho, K. Predicting the morphology of perovskite thin films produced by sequential deposition method: a crystal growth dynamics study. *Chem. Mater.* **29**, 1165–1174 (2017).
36. Du, J. S. et al. Halide perovskite nanocrystal arrays: multiplexed synthesis and size-dependent emission. *Sci. Adv.* **6**, eabc4959 (2020).
37. Weinberg, M. C., Birnie, D. P. III & Shneidman, V. A. Crystallization kinetics and the JMAK equation. *J. Non Cryst. Solids* **219**, 89–99 (1997).
38. Sinha, I. & Mandal, R. K. Avrami exponent under transient and heterogeneous nucleation transformation conditions. *J. Non Cryst. Solids* **357**, 919–925 (2011).
39. Jung, M. et al. Perovskite precursor solution chemistry: from fundamentals to photovoltaic applications. *Chem. Soc. Rev.* **48**, 2011–2038 (2019).
40. Bai, R. et al. Molecular dynamics simulation of the diffusion behavior of water in poly (vinylidene fluoride)/silica hybrid membranes. *RSC Adv.* **5**, 57147–57154 (2015).
41. Liu, D. et al. Universal growth of perovskite thin monocrystals from high solute flux for sensitive self-driven X-ray detection. *Nat. Commun.* **15**, 2390 (2024).
42. Gibbs, J. W. On the equilibrium of heterogeneous substances. *Trans. Conn. Acad. Arts Sci.* **3**, 108–248 (1876).
43. Perez, V., Chang, B. J. & Stelzer, E. Optimal 2D-SIM reconstruction by two filtering steps with Richardson-Lucy deconvolution. *Sci. Rep.* **6**, 37149 (2016).

Acknowledgements

Kebin Shi discloses support for the research of this work from Funders of Guangdong Major Project of Basic and Applied Basic Research (2020B0301030009), National Key Research and Development Program of China (2022YFF0712500), National Natural Science Foundation of China (92150301, 91750203, 12041602, 91850111). Lige Liu discloses support for the research of this work from Funders of National Natural Science Foundation of China (12004012) and China Postdoctoral Science Foundation (2020M680230). Dashan Dong discloses support for the research of this work from Funders of National Natural Science Foundation of China (12004013), National Key Research and Development Program of China (2022YFC3401100), and China Postdoctoral Science Foundation (2020M680220). This work was also supported by High-performance Computing Platform of Peking University. We also thank Yunan Gao from Peking University with the help on paper writing.

Author contributions

Kebin Shi and Haizheng Zhong devised the idea of research on crystallization of perovskite nanocrystals at single-particle level using super-resolution fluorescence imaging. Kebin Shi, Xiaoshuai Huang and Liangyi Chen provided platforms of the optical imaging system. Lige Liu designed and performed the experiments and analyzed fluorescence imaging data. Dashan Dong processed the fluorescence images. Zhiwei Long help to conduct the in situ spectra measurements. Wanxue Wei provided help with the theoretical calculations. Chang Sun and Wei Liu advised on the experimental design. Lige Liu, Haizheng Zhong and Kebin Shi wrote the manuscript with input from all the co-authors.

Competing interests

The authors declare no competing interests.

Additional information

Supplementary information The online version contains supplementary material available at https://doi.org/10.1038/s41467-025-60826-x.

Correspondence and requests for materials should be addressed to Haizheng Zhong or Kebin Shi.

Peer review information *Nature Communications* thanks Ou Chen and the other anonymous reviewer(s) for their contribution to the peer review of this work. A peer review file is available.